Published in final edited form as:
ACS Appl Mater Interfaces. 2009 June 24; 1(6): 1292–1304. doi:10.1021/am9001698.

Dendritic Phosphorescent Probes for Oxygen Imaging in Biological Systems

Artem Y. Lebedev[†], **Andrei V. Cheprakov**[‡], **Sava Sakadžić**[§], **David A. Boas**[§], **David F. Wilson**[†], and **Sergei A. Vinogradov**[*,†]
Department of Biochemistry and Biophysics, University of Pennsylvania, Philadelphia, Pennsylvania 19104, Department of Chemistry, Moscow State University, Moscow, Russia, and Martinos Center for Biomedical Imaging, Massachusetts General Hospital/Harvard Medical School, Charlestown, Massachusetts 02129

Abstract

Oxygen levels in biological systems can be measured by the phosphorescence quenching method using probes with controllable quenching parameters and defined biodistributions. We describe a general approach to the construction of phosphorescent nanosensors with tunable spectral characteristics, variable degrees of quenching, and a high selectivity for oxygen. The probes are based on bright phosphorescent Pt and Pd complexes of porphyrins and symmetrically π-extended porphyrins (tetrabenzoporphyrins and tetranaphthoporphyrins). π-Extension of the core macrocycle allows tuning of the spectral parameters of the probes in order to meet the requirements of a particular imaging application (e.g., oxygen tomography versus planar microscopic imaging). Metalloporphyrins are encapsulated into poly(arylglycine) dendrimers, which fold in aqueous environments and create diffusion barriers for oxygen, making it possible to regulate the sensitivity and the dynamic range of the method. The periphery of the dendrimers is modified with poly(ethylene glycol) residues, which enhance the probe's solubility, diminish toxicity, and help prevent interactions of the probes with the biological environment. The probe's parameters were measured under physiological conditions and shown to be unaffected by the presence of biomacromolecules. The performance of the probes was demonstrated in applications, including in vivo microscopy of vascular pO_2 in the rat brain.

Keywords

phosphorescence; oxygen; porphyrins; dendrimers; quenching; imaging

INTRODUCTION

Optical sensors and imaging agents are rapidly developing areas of research in functional macromolecular materials (1). Sensors based on dendrimers attract special interest because,

*vinograd@mail.med.upenn.edu.
[†]University of Pennsylvania.
[‡]Moscow State University.
[§]Massachusetts General Hospital/Harvard Medical School.

Note Added after ASAP Publication. In the version of this paper published on the Web on June 1, 2009, the author named Sakadzic was misspelled, due to a production error. The spelling of this author's name that has been published on the web on June 5, 2009, is correct.

Supporting Information Available: Detailed description of synthetic procedures, ^{1}H and ^{13}C NMR, MALDI-TOF, absorption and emission spectra, Stern–Volmer oxygen quenching plots, and details of biological experiments. This material is available free of charge via the Internet at http://pubs.acs.org.

among all types of synthetic polymeric carriers, dendrimers offer the unique advantage of molecular monodispersity (2). In imaging, dendritic polymers are typically used for signal amplification or for the construction of controlled microenvironments by way of dendritic encapsulation (3,4). If an optically active motif is placed inside a dendrimer, the latter forms a protective cage, preventing physical contacts of the core with macromolecular objects and shielding it from small-molecule quenchers in the environment. Optical probes for biological imaging of oxygen present an important example of the encapsulating capability of dendrimers, which play a key role in the construction of these practically useful materials.

Oxygen-dependent quenching of phosphorescence (5) is an optical method for oxygen sensing in biological systems (6,7). Applications of the technique range from local "point" measurements to planar 2D imaging (8) to high-resolution microscopy (9) and near-infrared 3D tomography (10). Phosphorescence quenching offers excellent specificity, sub-millisecond temporal response, high sensitivity, and relative simplicity of implementation, complementing and in many ways surpassing other oximetry methods (11–15).

In phosphorescence quenching, probes are the only invasive component of the measurement scheme, and their design is the key to applicability of the method. Early oxygen probes were based on simple water-soluble derivatives of palladium porphyrins (5). These chromophores had to be prebound to bovine serum albumin in order to enhance their solubility and to prevent interactions of the porphyrins with biological molecules. Prebinding was also important because water-soluble porphyrins, modified with either ionic groups (SO_3^-, CO_2^-, NH_3^+) or neutral residues, e.g., oligo(ethylene glycols) (16), are prone to aggregation. Moreover, when injected systemically, they bind to biological targets and become heterogeneously distributed throughout the tissue. Local environments of probe molecules in different tissue microcompartments are highly heterogeneous, and as a result, the response of phosphorescence to oxygen cannot be interpreted quantitatively. Binding to albumin makes it possible to partially overcome these limitation, but a number of problems arise as a result of the use of an exogenous protein, which constitutes a part of the injected material.

Introduction of polyglutamic phosphorescent probes (17) (in the literature known as Oxyphors R2 and G2) (18) eliminated the necessity of prebinding porphyrins to foreign albumin because polyglutamic branches rendered highly water-soluble materials. Still, polyglutamic probes required the endogenous albumin because only albumin complexes were suitable for measurements in the physiological oxygen range (vide infra). Consequently, oxygen measurements could be performed only in albumin-rich environments (blood plasma), while incomplete albumin binding, e.g., at the higher probe concentrations needed to increase the signal level, could lead to measurement ambiguity (19).

A more comprehensive design of a molecular sensor for oxygen would entail construction of a well-defined microenvironment around the phosphorescent chromophore with the purpose of isolating it from interactions with biological molecules. Dendritic encapsulation arguably provides the most straightforward way for the construction of monodisperse, well-defined molecular jackets around luminescent centers, although other approaches have been proposed in the literature (20). In this paper, we present a comprehensive design of phosphorescent oxygen nanosensors for biological environments and describe a family of dendritic oxygen probes with excitation bands spanning the entire UV–vis–near-infrared (NIR) spectrum.

RESULTS AND DISCUSSION

Probe Parameters

Molecular oxygen, a triplet molecule in the ground state ($O_2{}^3\Sigma_g^-$), is able to react with excited molecules in the environment, quenching their luminescence (21). Collisional quenching is

much less probable on the time scale of singlet excited states (nanoseconds) than of triplet states (microseconds to milliseconds), making phosphorescence much more sensitive to oxygen than fluorescence. Assuming a large excess of oxygen relative to the concentration of triplet emitters, a condition typically met in biological experiments, the dependence of the phosphorescence intensity and lifetime on the oxygen concentration follows the Stern–Volmer relationship

$$I_0/I=\tau_0/\tau=1+K_{sv}[O_2] \quad (1)$$

where I and τ are the phosphorescence intensity and lifetime at the oxygen concentration ($[O_2]$) and in the absence of oxygen (I_0 and τ_0) and K_{SV} is the Stern–Volmer quenching constant. In practice, using lifetime τ as the analytical signal for $[O_2]$ is more convenient because the lifetime is independent of the probe distribution, provided the chromophore is in the same molecular environment.

We express the oxygen content in the units of pressure (mmHg) rather than concentration (M) (22) because in the majority of experiments the partial pressure of oxygen (pO_2) is the experimental parameter that is actually controlled. We assume that the Henry's law holds in the physiological range of the oxygen concentrations: $[O_2] = \alpha pO_2$, where α is the oxygen solubility coefficient (M $mmHg^{-1}$). Considering $K_{SV} = k_2\tau_0$, where k_2 is the bimolecular rate constant for the quenching reaction, eq 1 can be rewritten as

$$1/\tau=1/\tau_0+k_q pO_2 \quad (2)$$

where $k_q = \alpha k_2$ and has units of $mmHg^{-1}\ s^{-1}$.

Equation 2 contains two probe-specific parameters: constant k_q and lifetime τ_0. Their interplay defines the sensitivity and dynamic range of the method. It is desirable that the measurement parameter, phosphorescence lifetime τ, spans the largest possible interval of values throughout the range of analyte concentrations, assuring the highest possible measurement resolution. To quantify the dynamic range of lifetimes, it is convenient to define parameter $R = (\tau_0 - \tau_{air})/\tau_0$, where τ_0 ($pO_2 = 0$ mmHg) and τ_{air} ($pO_2 = 159.6$ mmHg) are the maximal and minimal values of the phosphorescence lifetimes in physiological experiments. Another important parameter is the signal-to-noise ratio, which is always higher for probes with larger emission quantum yields, assuming the same emission spectra.

Triplet lifetimes of palladium porphyrins in deoxygenated solutions at ambient temperatures are in the range of hundreds of microseconds, and their phosphorescence quantum yields are typically 0.05–0.1 (23). Constants k_q for "unprotected" metalloporphyrins in aqueous solutions are ~3000 $mmHg^{-1}\ s^{-1}$ ($1.9 \times 10^9\ M^{-1}\ s^{-1}$). Given such high quenching constants, the lifetimes and quantum yields of palladium porphyrins become extremely low already at low oxygen concentrations because of excessive quenching (see Figure S22 in the Supporting Information). Thus, in spite of the overall very high signal dynamic range (R ~ 0.99), palladium porphyrins can be useful only in a very low pO_2 range, probably not higher than ~5 mmHg.

For platinum porphyrins, lifetimes τ_0 are typically tens of microseconds and their quantum yields are 0.10–0.25 (23,24). As a result, platinum porphyrins can be used up to about ~50 mmHg of pO_2, but above that limit, probe quantum yields also become low and lifetimes change only weakly, causing poor analyte resolution and low sensitivity. Moreover, if quenching constants were to decrease, which is inevitable upon binding of the probes to biological

macromolecules, probes with short lifetimes would become very poorly sensitive to small changes in the analyte concentration [$R \sim 0.5$ for platinum porphyrins; compare to $R \sim 0.02$ for $Ru(bpy)_3$-like complexes (25)].

For higher sensitivity, probes with greater τ_0's are clearly preferred, but only if their phosphorescence changes gradually instead of being highly quenched already at low oxygen concentrations. Such an adjustment of the sensitivity can be achieved by tuning constants k_q. For example, at $k_q \sim 100\ mmHg^{-1}\ s^{-1}$, phosphorescence of palladium porphyrins would change more gradually, permitting measurements even at air saturation, but the dynamic range would still be quite high ($R \sim 0.9$; see Figure S22 in the Supporting Information). In some cases, when the signal strength is particularly critical, probes with higher quantum yields (PtP) still would be more useful even at the expense of the sensitivity, especially if only qualitative information about pO_2 is required.

Overall, it is clear that control over the values of quenching constants k_q and, most importantly, the ability to keep them unaltered is the key to accurate oxygen measurements. For the majority of phosphorescent chromophores, diffusion of oxygen can be considered the rate-limiting step for the quenching reaction (21). Therefore, through alteration of oxygen diffusion in the local environment of phosphorescent chromophores, constants k_q can be regulated.

Considering the above criteria, a molecular design emerges that comprises a bright phosphorescent chromophore with sufficiently long triplet lifetime τ_0 and a protective jacket, whose purpose is to constrain oxygen diffusion in the local environment of the chromophore. The periphery of the probe must be hydrophilic and inert in order to prevent interactions of the probe with components of the biological system (e.g., biomacromolecules and cellular membranes).

Phosphorescent Chromophores

Relatively few chromophores exhibit bright (26) phosphorescence at ambient temperatures. Among them, α-diimine complexes of Ru, Ir, and some other transition metals (7a), cyclometalated complexes of Ir and Pt (27), and Pt and Pd complexes of porphyrins and related tetrapyrroles (5,23,28,29) have been used in oxygen sensing, although some other systems have been proposed (30).

For tissue applications, it is desirable that probes posses absorption bands in the NIR region. It has been shown that lateral π-extension of platinum and palladium porphyrins by annealing of their pyrrole residues with external aromatic rings renders chromophores with dramatically red-shifted absorption bands and strong room-temperature phosphorescence (31–33,28). Structures, absorption and emission spectra of palladium tetraarylporphyrin (PdP), palladium tetraaryltetrabenzoporphyrin (PdTBP), and palladium tetraaryltetranaphthoporphyrin (PdTNP) are shown in Figure 1 (34). Spectra of Pt complexes are very similar in shape but are slightly blue-shifted (10–15 nm) compared to those of the Pd counterparts (see Table 2). The three basic porphyrin types, P, TBP, and TNP, are designated in Figure 1 as **1**–**3**, respectively. In this study, we used *meso*-tetraarylporphyrins, where aryl (Ar) = $3,5(RO_2C)_2C_6H_3$. [To distinguish between different groups R and metals (Pt and Pd), prefixes and endings indicating the porphyrin types are added to the numbers. For example, the Pt complex of TBP with butoxycarbonyl substituents is abbreviated as Pt-**2**-OBu.]

In platinum and palladium porphyrins, $S_1 \rightarrow T_1$ intersystem crossing is the predominant pathway of deactivation of the singlet excited states (S_1) (23), and the resulting triplet states are typically highly emissive (phosphorescent). In regular (nonextended) porphyrins, macrocycle deviations from planarity dramatically enhance the competing nonradiative triplet decay and quench phosphorescence (35). In contrast, platinum and palladium *meso*-

tetraaryltetrabenzoporphyrins (TBPs), although highly nonplanar (31), phosphoresce with high quantum yields (36). Palladium (31d) and platinum tetraaryltetranaphthoporphyrins (Figure 2 and Supporting Information) (33b) are also nonplanar and, in addition, have much narrower T_1–S_0 gaps (Table 1). Nevertheless, they still phosphoresce, although weaker than TBPs and regular porphyrins. The emission spectra in Figure 1b are scaled to reflect the relative phosphorescence quantum yields, and the complete photophysical data for the chromophores are summarized in Table 1.

Taken together, the absorption bands of Pt and Pd Ps, TBPs, and TNPs cover practically the entire UV–vis–NIR range, presenting multiple opportunities for excitation. The absorption *Q* bands of TBPs and TNPs are shifted to the red, i.e., into the region between ~630 and ~950 nm, where the absorption of endogenous chromophores is significantly lower (38). The oscillator strengths of these bands are extremely high, making TBPs and TNPs especially well-suited for optical tomographic applications (10). Excitation in the visible region (near 500 nm), featured by regular PtPs and PdPs, is useful in planar wide-field imaging (vide infra), where the less diffuse nature of excitation serves to improve the spatial resolution. In addition, absorption near 500 nm overlaps with the emission of many two-photon chromophores, which is useful in the construction of fluorescence resonance energy-transfer enhanced probes for two-photon oxygen microscopy (9).

An important feature of porphyrin-based probes is their record-high phosphorescence Stokes shifts achievable via excitation at the Soret bands (e.g., 9329 cm^{-1} for PdP). Efficient $S_2 \rightarrow S_1$ internal conversion (39), combined with extremely high extinction coefficients of S_0–S_2 transitions (~3×10^5 M^{-1} cm^{-1}), makes this pathway superior to the direct S_0–S_1 excitation in those cases when near-UV radiation can be sustained by the object.

Porphyrins with *meso*-3,5-dicarboxyphenyl groups were used in this study as cores for the dendrimers (Figure 1). Regular tetraarylporphyrins were synthesized by the Lindsey method (40) using 3,5-butoxycarbonylbenzaldehyde. The same aldehyde was used in the synthesis of π-extended analogues, as depicted in Scheme 1iii–v.

The pathway shown in Scheme 1 is based on the modified Barton–Zard reaction (i) (41), used to generate pyrroles annealed with exocyclic nonaromatic rings, followed by the macrocycle assembly by the Lindsey method (vi) (40), metal insertion into the resulting porphyrins (vii), and oxidative aromatization (viii) into the target π-extended macrocycles (31). Pt and Pd complexes were obtained in excellent purity and good overall yields. The core porphyrins are also referred to below as G0 dendrimers. The footnote to Scheme 1 contains references to the sources where the corresponding protocols were developed and/or used in similar syntheses. Our modifications and improvements of these procedures are detailed in the Supporting Information.

Dendritic Cages

Dendritic attenuation of quenching has been documented in a number of studies, where quenchers had different sizes and charges and the quenching processes themselves had different mechanisms (e.g., electron transfer vs energy transfer) (42). If a chromophore is encapsulated inside a dendrimer, the latter forms a protective cage, preventing physical contacts of the core with macromolecular objects in the environment. However, protecting the chromophore from collisions with small molecules is not as straightforward because the latter can effectively diffuse through the body of the dendritic matrix.

It is important to realize that quenching constant k_q in eq 2 is a product of the quencher concentration and the diffusion coefficient, which are both affected by the chromophore environment. If the solubility of oxygen in the solvent (e.g., water) is lower than that in the

bulk of the dendrimer, the latter can serve as a "concentrator" for oxygen. Still, a decrease in the rate of oxygen diffusion can effectively offset an increase in its local concentration, thus lowering the apparent constant k_q. Hydrophobic dendritic branches fold in polar environments (e.g., water), and as a result, their mobility becomes restricted, preventing oxygen molecules from freely reaching the phosphorescent core (43). A similar situation occurs in proteins (44). Notably, the density of the folded dendritic branches may be lower than that of the bulk solvent, and the solubility of oxygen in the folded dendrimer might be higher than that in the solvent; nevertheless, the constrained dynamics of the branches affects the diffusion much more than the density and/or the solubility.

Dendrimer dynamics is influenced by the interactions of the branches with the solvent. In "good" solvents, the mobility is higher, and oxygen diffusion to the core is attenuated less than in "bad" solvents. Similarly, for the same solvent, dendrimers with more solvent-compatible composition limit oxygen access much less than less compatible dendrimers. In particular, dendrimers composed of aromatic motifs are most effective in shielding porphyrins from oxygen in aqueous solutions (43).

Among many dendrimers with flexible aromatic skeletons, dendritic poly(arylglycine) (AG) dendrons (45) (Scheme 2) are especially well-suited for the construction of phosphorescent oxygen probes. AG dendrons offer the advantage of inexpensive starting materials, simplicity of synthesis, and chromatography-free purification. Focal amino groups on AG dendrons complement carboxyls on the core porphyrins, whereas terminal carboxyls on the dendrons provide multiple opportunities for functionalization. AG dendrons (Scheme 2) of three successive generations (G1–G3) were used in this work for modification of platinum and palladium porphyrins and π-extended porphyrins. The resulting dendritic compounds are abbreviated as follows:

For dendrons: **X-AG^{n}R**, where AG denotes the dendritic arylglycine skeleton, *n* is the dendrimer generation number, X is the focal functionality, and R is the terminal group. For example, a butyl-ester-terminated AG dendron of generation 2 with a Boc-protected amino group at the focal point is abbreviated as BocNH-AG^{2}OBu.

For dendrimers: **C-(AG^{n}R)$_m$**, where C denotes the dendrimer core, AG denotes the dendritic arylglycine skeleton, *n* is the generation number, R is the terminal group, and *m* is the number of dendritic wedges attached to the core. For example, a generation 2 AG dendrimer consisting of a PdTBP core and eight AG dendrons terminated by carboxyl groups is abbreviated as Pt-**2**-(AG^{2}OH)$_8$.

The synthesis in Scheme 2 makes use of the Fischer haloacyl halide method to generate building blocks **4** and **5** (45). The following assembly relies on peptide coupling reactions, employing CDMT/NMM and HBTU/DIPEA (see the Scheme 2 footnote for abbreviations) and permitting the synthesis of dendrons **6** and **7** in high purity and yield. The AG dendrons can be produced in multigram quantities and stored for long periods of time without detectable decomposition.

Poly(ethylene glycol) (PEG) Layer

Special requirements to probes for medical imaging applications include the lack of toxicity and excretability from the blood upon completion of imaging. Globular uncharged molecules with molecular weights between 1 and 15 kDa are usually excretable by the kidney (46). If a probe satisfies this criterion and remains confined to the intravascular space (does not diffuse out of the blood vessels), it is likely to be removed from the blood by kidney-mediated dialysis, and the possibility of long-term toxicity effects can be avoided.

One way to eliminate interactions of dendritic probes with biological macromolecules and to avoid toxicity is to modify their termini with PEG residues. PEGylation of macromolecular compounds for drug delivery and related applications (e.g., artificial blood) is a widely known strategy (47), including PEGylation of dendrimers (48). Peripheral PEG groups on porphyrin dendrimers successfully eliminate interactions of the probes with proteins, while keeping the probes highly hydrophilic. Although PEG residues themselves also contribute to the attenuation of oxygen quenching, their effect is small compared to that of the hydrophobic branches (43). In addition, the effect of PEGs on the accessibility of the cores to oxygen saturates with an increase in the length of linear poly(ethylene oxide) chains (49). As a result, probe molecules of virtually any size can be generated without significantly changing the quenching properties.

Probe Assembly

Synthetic assembly of the dendritic probes consists of attachment of the dendrons to the cores, hydrolysis of the peripheral ester groups, and modification of the peripheral carboxyls with PEG residues. Each step of this sequence was optimized in order to ensure maximal yields and monodispersity of the probes. Scheme 3 shows the complete reaction sequence as well as the structure of a selected probe molecule, Pd-**2**-$(AG^2OPEG)_8$. The table in Scheme 3 enumerates the final probe molecules of the general formula **C**-$(AG^2OPEG)_8$.

Using CDMT as a coupling reagent (50), G1 dendritic branches (**5**) were attached to the core porphyrins, yielding perfect dendrimers **C**-$(AG^1OBu)_8$ in 90–95% yield. These dendrimers could be readily purified from an excess of **5** by washing the crude mixtures with ethanol.

However, CDMT chemistry was not successful in the case of G2 and G3 dendrimers. Matrix-assisted laser desorption ionization time-of-flight (MALDI-TOF) analysis of the reaction mixtures revealed the presence of dendrimers with four-to-eight AG^2OBu branches. Additional experiments confirmed that lower-molecular-weight peaks in the MALDI spectra were not caused by fragmentation (see the Supporting Information).

Among several established peptide-coupling systems (including $[(Me_2N)_2CF]^+PF_6^-$, DCC, CDI, uronium-based reagents HBTU (*O*-benzotriazole-*N*,*N*,*N*′,*N*′-tetramethyluronium hexafluorophosphate) and HATU (2-(1*H*-7-azabenzotriazol-1-yl)-1,1,3,3-tetramethyluronium hexafluorophosphate) (51), uronium reagents proved to be superior for the complete modification of porphyrins with AG^2 dendrons **6**. However, when used under the originally proposed conditions, they still produced mixtures containing imperfect dendrimers. We have found that the single most important parameter with respect to complete derivatization of porphyrins with AG dendrons is the choice of solvent. Porphyrin octacarboxylic acids are soluble only in polar aprotic solvents [e.g., dimethylformamide (DMF), dimethylacetamide (DMA), *N*-methylpyrrolidone (NMP), and dimethyl sulfoxide (DMSO)], and NMP was found to be the optimal choice. Possibly, porphyrins are much less aggregated in NMP, and NMP contains much fewer free-amine impurities than DMF or DMA. Small amine molecules effectively compete with bulky AG dendrons in the coupling reaction, as evidenced, for example, by the presence of peaks corresponding to **C**-$(AG^2OBu)_7NMe_2$ in the MALDI spectra of reactions carried out in DMF. Notably, reaction intermediates bearing eight activated carboxyl groups on the porphyrin core are highly unstable at room temperature. Reactants (AG dendrons) need to be added to the mixtures immediately following the addition of DIPEA.

Complete derivatization of porphyrins required a ~1.5 molar excess of dendron **6**. The excess reagent was removed using isothiocyanate-modified resin (Sigma-Aldrich), designed specifically to scavenge molecules with free amino groups. Thus, prepurified dendrimers were subjected to size-exclusion chromatography on SX-1 beads (Biorad) using tetrahydrofuran (THF) as a mobile phase.

As expected, modification of porphyrins with AG^3 dendrons **7** proved to be extremely challenging. So far, the best result obtained was a 2:2:1 mixture of dendrimers with six, seven, and eight AG^3 branches, respectively, attached to Pt-**1**-OH. Fortunately, from a practical point of view, modification of the cores with G2 dendrons was sufficient for attenuation of oxygen sensitivity (vide supra), whereas slightly imperfect G3 dendrimers were adequate for understanding the trends of the dendrimer behavior at higher generations.

In spite of the presence of multiple butyl ester groups, solubility of the porphyrin AG dendrimers in common solvents, such as CH_2Cl_2, ether, acetone, and methyl and ethyl alcohols, was found to be quite limited; however, AG dendrimers are well-soluble in THF, DMSO, and pyridine. Each of the last three solvents is stable in the presence of alkali, permitting hydrolytic cleavage of the terminal esters under basic conditions. However, while attempting to use NaOH in THF/H_2O (50:1), we found that MALDI spectra of the reaction mixtures showed peaks with lower molecular masses than was expected for dendrimers polycarboxylic acids, likely because of the partial hydrolysis of anilides in the body of the dendrimer (52).

In order to remove the peripheral butyl groups without affecting the dendrimer integrity, a two-step scheme was devised. At first, poly(butyl ester) dendrimers were treated with NMe_4OH (~5 mM) in DMSO/MeOH over a 20–60 min period, followed by solvent removal and subsequent hydrolysis in 0.1 N aqueous NaOH overnight. As a result, pure monodisperse dendrimer carboxylic acids could be isolated in 80–95% yield. Importantly, when applied to crude mixtures of **C**-$(AG^2OBu)_8$ (Scheme 3), contaminated with unreacted dendrons **6**, this two-step sequence yielded completely pure acids **C**-$(AG^2OH)_8$, containing no traces of dendrons H_2N-AG^2OH. From a practical point of view, this result is extremely useful because it made it possible to avoid chromatographic purification of the butyl ester dendrimers and thus significantly improve the overall yields. For example, Pt-**1**-$(AG^2OH)_8$ could be obtained without purification in 81% yield starting from Pt-**1**-OH and **6**.

At the last stage, the peripheral carboxyl groups on the dendrimers were esterified with monomethoxyoligo(ethylene glycol) residues (av MW 350) in order to obtain water-soluble neutral probes. Esterification was carried out using the earlier developed DCC/HOBt chemistry (53). One important practical result of this work is that a convenient work-up procedure after the esterification reaction was developed to entirely avoid chromatographic purification. It was found that, by simple reprecipitation of PEGylated dendrimers from THF upon the addition of diethyl ether, pure PEGylated dendrimers could be obtained. The yields of PEGylation varied in the range of 50–65%. Judging from the MALDI spectra, 95–100% of the carboxyl groups were converted to the PEG esters.

Photophysical Properties

The photophysical data for the phosphorescent probes are summarized in Table 2. Spectra of the three selected probes based on platinum porphyrins with changing degrees of π-extension are shown in Figure 3 (54).

Optical properties of the dendrimers in the UV–vis–NIR range are mostly determined by their porphyrin cores (see Figure 1 for comparison). The absorption bands of all G2 (**9** and **12**–**14**) and G3 (**11**) dendrimers in aqueous solutions are very close to those of the parent porphyrins (Pt-**1**-OBu, Pt-**2**-OBu, and Pt-**3**-OBu) in PhCN, suggesting that the cores are buried inside the dendritic matrix. In contrast, the Soret bands of the G1 dendrimer (8) and of the unprotected porphyrin Pt-**1**-OPEG (8), also in aqueous solutions, are blue-shifted by about 15 nm compared to those of **9** and **11** (Figure 4a).

In addition, the absorption spectrum of the G1 dendrimer **8** was found to drift considerably in time. If registered immediately after dissolution, the Soret band revealed a shoulder (as shown

in Figure 4a); however, over about 1 h, this shoulder gradually disappeared. Typically, such behavior is associated with porphyrin aggregation in aqueous solutions.

The trends in the emission spectra generally reflect those in the absorption. However, the emission spectra of more aggregated and more solvent-exposed G0 and G1 compounds (Pt-**1**-OPEG and **8**) were found to be shifted to the red, instead of to the blue, relative to the spectrum of the parent porphyrin (Pt-**1**-OBu) in PhCN. The emission maxima of all probes (Figure 4b) fall into the tissue NIR window, although phosphorescence of the PtTNP-based dendrimer (14) occurs close to its red border. Compared to the platinum porphyrin dendrimers (e.g., **9** and **12**), Pd counterparts (10 and 13) exhibit lower quantum yields and significantly longer lifetimes, reflecting the behavior of the parent porphyrins (Tables 1 and 2).

In aqueous solutions, the phosphorescence lifetimes (τ_0) and the quantum yields (φ) of the probes increase with an increase in the dendrimer generation (see, for example, compounds Pt-**1**-OPEG, **8**, **9**, and **11**). The quantum yields appear to grow consistently from G0 to G3 dendrimers, although between G2 and G3, the growth somewhat slows down. Separate studies will be required to understand this phenomenon, but the explanation might involve limited quenching of the triplet state by the solvent in larger dendrimers and/or a decrease in the vibrational flexibility of a porphyrin as it becomes more and more confined within the folded dendritic matrix. In porphyrins, vibrations are known to affect the magnitude of spin–orbit coupling (21,35,36); therefore, tight confinement could decrease nonradiative $T_1 \rightarrow S_0$ relaxation and benefit the radiative channel.

Phosphorescence Quenching

The effect of dendritic attenuation of phosphorescence quenching by oxygen in the series of platinum porphyrin dendrimers is shown in Figure 5a, and the respective values of the quenching constants (k_q) and lifetimes (τ_0) are summarized in Table 2. These data were obtained by simultaneously measuring phosphorescence lifetimes and pO_2, using a high-precision oxygen electrode system, while gradually replacing oxygen in the solution by argon (see the Supporting Information).

As expected, the slopes of the Stern–Volmer plots decrease significantly with an increase in the dendrimer generation. Overall, between G0 (Pt-**1**-OPEG) and G3 (11), the quenching rate drops by nearly 20 times. The quenching constants and lifetimes of palladium porphyrin G2 dendrimers (**10** and **13**) appear to be well-suited for biological oxygen measurements, and the probes reveal a good dynamic range and excellent sensitivity (e.g., $R \approx 0.9$ for **13** at 37 °C). Overall, the magnitude of the attenuation effect is similar to that reported earlier for different polyaromatic dendrimers (17,42c).

Data in Table 2 reveal that the relative decrease in the quenching efficiency levels off at higher generations. For example, between G1 and G2, the quenching rate drops by more than 4 times, whereas in going from G2 to G3, the decrease is about 2 times smaller (55). This saturation of the dendritic effect can be rationalized by recalling that constants k_q reflect the rate of oxygen diffusion in the close vicinity of the porphyrin center. Attachment of G1 dendrons dramatically changes the composition of the medium around the porphyrin, from pure solvent to a “mixture” of the solvent and the dendrons. The difference in the medium near the core when going from G1 to G2 dendrimers is still substantial: larger G2 dendrons are able to expel more solvent molecules from the porphyrin environment. However, when the dendrimer is already large, the addition of distant peripheral layers has little effect on the composition in the immediate vicinity of the porphyrin. Notably, the fact that oxygen diffusion is the rate-limiting step in the overall quenching reaction manifests itself by the close proximity of the k_q values for the probes of the same dendritic generation but with different porphyrin as cores (**9**, **10**, and **12**–**14**), which supports the above model.

One of the most practically important results of this work is that oxygen quenching constants k_q of the probes and their lifetimes τ_0 are indeed completely insensitive to the presence of biological macromolecules. Oxygen titrations performed in the presence of bovine serum albumin clearly show that the neutral PEG layer on the dendrimer prevents binding of the probe to albumin (Table 2). In contrast, the quenching constants of dendrimers without PEG layers usually change by several fold in the presence of albumin. To further investigate whether the probes can be used directly in biological experiments, we titrated PdTBP-based dendrimer **13** in the rat blood plasma at physiological temperature (36.9 °C). To avoid coagulation, the blood was treated with a small amount of heparin, and the red blood cells were removed by centrifugation in order to facilitate equilibration of the solution with air (56). The resulting Stern–Volmer plot was superimposed on the plot obtained at identical conditions (36.9 °C) in an aqueous phosphate buffer at pH 7.4 containing no proteins (Figure 5c). The obtained result clearly demonstrates that the probe constants are unaffected by the blood plasma components.

Additional experiments revealed that phosphorescence lifetimes measured at constant temperatures and oxygen concentrations did not change over long periods of time (days) (Figure 5b, inset). The solutions of the probes showed no traces of decomposition (change in absorption) when measurements were performed as frequently as every 1 min over 2–3 day periods. Altogether, these results suggest that dendritically protected probes are superior to all previously described molecular oxygen sensors and can be directly applied to biological oxygen measurements and imaging.

Biological Experiments

To illustrate the performance of the probes, we performed two experiments: (1) measurements of the oxygenation of the mouse brain because it is affected by changes in the cerebral blood flow; (2) wide-field microscopic imaging of oxygen in intact rat brain.

The schematic of the first experiment is shown in Figure 6. An anesthesized mouse was laid on its back, and three optical fibers were positioned next to its skull. The left and right fibers were used for excitation (635 nm LED), while the bottom fiber served to collect the phosphorescence (57). PdTBP-based probe **13** was injected into the vein and distributed throughout the blood within seconds. Excitation pulses were delivered, in turn, by the left and right fibers, thus sampling independently through the two brain hemispheres, as shown by the banana-like shapes in the figure.

The time traces of intravascular pO_2 in both right and left hemispheres are shown in the graph (Figure 6). As measurements progressed, the carotid arteries were occluded (point 1), leading to ischemic hypoxia (e.g., hypoxia caused by an insufficient blood flow). This change in oxygenation was instantly reflected by the phosphorescence signals in both channels. When the arteries were released (point 2), the brain rapidly reoxygenated, initially to higher pO_2 values than that in the beginning of the experiment. In the next episode, only one artery was occluded (point 3), which, as expected, was followed by a drop in the pO_2 value in the corresponding brain region (left), whereas the blood flow in the opposite artery increased in order to compensate for the loss of the overall oxygenation. Eventually, the pO_2 values in both hemispheres equilibrated, after which the occlusion (point 4) and reperfusion (point 5) of both arteries were repeated. This experiment demonstrates the functionality of the probe and shows that when using excitation at 635 nm, oxygenation can be measured in deep layers of the tissue, making it possible to utilize dendritic tetrabenzoporphyrin-based probes in tomographic imaging (10).

The second experiment was designed to demonstrate applicability of the probes in high-resolution microscopic imaging. It was conducted as a part of the studies devoted to elucidating the brain hemodynamic response to propagation of the cortical spreading depression (CSD) in

rats (58). The CSD is a self-propagating wave of cellular depolarization that travels with a speed of 2–4 mm min^{-1} through the cortex. The CSD has been implicated in migraines (59) and in progressive neuronal injuries after stroke and head trauma (60).

The position of the cranial window and a photograph of the cortical vasculature are shown in Figure 7a. Palladium porphyrin dendrimer **10**, excitable in the visible range, was used in this experiment. Our imaging setup consisted of an in-house-constructed up-right microscope with a cooled CCD camera as an imaging detector and a frequency-doubled Nd: YAG pulsed laser as an excitation source (see the Supporting Information). A series of intensity images were taken at different delays following the excitation flash. Fitting these images with exponentials in each pixel produced the phosphorescence lifetime image, which was converted into the pO_2 image using the Stern–Volmer relationship.

A CSD wave was initiated at the beginning of the experiment by injecting the KCl solution through a small opening in the frontal bone. The high-resolution integrated intensity image (Figure 7b), taken prior to the arrival of CSD, clearly shows that the probe is confined to the blood vessels on the cortical surface, reporting specifically on vascular pO_2. The corresponding pO_2 map is shown in Figure 7c. pO_2 values at locations distant from major arteries largely represent venous blood oxygenation because of a much smaller volume and substantially higher oxygen quenching in the arterial blood relative to the venous blood. On the basis of pO_2 values in Figure 7c, arteries and veins in the cortical blood vessel network can be easily distinguished. Notably, the blood in the draining vein apparent on the right side of the cranial window has a lower pO_2 value because of the arrival of a CSD wave.

The above experiments convincingly demonstrate the usefulness of the probes in physiological studies, where they allow the determination of absolute blood pO_2, which is essential for the analysis of the dynamic delivery of oxygen and building of a quantitative model of metabolism of the brain tissue.

CONCLUSION

The family of oxygen probes described in this account opens many new possibilities for noninvasive studies of tissue oxygenation and metabolism using phosphorescence quenching. Using a multilayered modular design, the probes can be tailored to the different modes of the phosphorescence imaging application, from point measurements to microscopy to tomography using infrared light. The probes can also be utilized in various in vitro assays and cell culture studies because they do not require repetitive calibrations and thus provide a superior alternative to oxygen electrodes and optodes.

The construction of the probes once again demonstrates the value of dendritic encapsulation as a method for active-site isolation and control of the chromophore environment. Encapsulation and protection make the phosphorescent probes directly applicable to oxygen measurements in all tissue microcompartments (intravascular, interstitial, and intracellular, assuming an adequate delivery pathway) without the need to perform in vivo calibration. This constitutes a significant step forward compared to the oxygen sensors used earlier.

Although limited interactions of the probes with biological macromolecules and chemical inertness are the necessary prerequisites of clinical applicability, a detailed investigation of the probe's biodistribution, toxicity (especially phototoxicity), and pharmacokinetics will need to be accomplished in order to evaluate their potential in clinical imaging. If required, the design described provides a versatile framework for the improvement and modification of the phosphorescent sensors and serves to further advance the phosphorescence quenching method.

EXPERIMENTAL SECTION

All solvents and reagents were obtained from commercial sources and used as received. Palladium porphyrins Pd-**1**-OBu and Pd-**1**-OH were synthesized as described previously (43). Column chromatography was performed on Selecto silica gel (Fisher) or aluminum oxide (neutral, Brockmann I, ~150 mesh, 58 Å). Preparative gel permeation chromatography was performed on S-X1 (Biorad) beads, using THF as a mobile phase, unless otherwise stated. ^{1}H and ^{13}C NMR spectra were recorded on a Bruker DPX-400 spectrometer. Mass spectra were obtained on a MALDI-TOF Voyager-DE RP BioSpectrometry workstation, using α-cyano-4-hydroxycinnamic acid as the matrix.

Detailed description of synthetic procedures, ^{1}H and ^{13}C NMR, MALDI-TOF, absorption and emission spectra and Stern-Volmer oxygen quenching plots can be found in Supporting Information.

Quartz fluorometric cells (Starna, Inc., 1 cm optical path length) were used in optical experiments. Optical spectra were recorded on a Perkin-Elmer Lambda 35 UV–vis spectrophotometer. Steady-state fluorescence and phosphorescence measurements were performed on a SPEX Fluorolog-2 spectrofluorometer (Jobin-Yvon Horiba), equipped with an infrared-enhanced R2658P PMT (Hamamatsu). Emission spectra were obtained using solutions with absorption at the excitation maximum of approximately 0.05 OD. Quantum yields of emission of all of the synthesized compounds were measured relative to the fluorescence of tetraphenylporphyrin $\varphi_{fl} = 0.11$ in deoxygenated C_6H_6 (37).

The system for oxygen titrations was described previously (43,61). Time-resolved phosphorescence measurements were performed using an in-house-constructed phosphorometer (57), modified for time-domain operation. For phosphorescence measurements, solutions were deoxygenated by argon bubbling (Airgas, grade 5.5), while monitoring changes in the phosphorescence lifetimes. Aqueous solutions were deoxygenated by a glucose/glucose oxidase/catalase enzymatic system (5) or by prolonged purging with argon.

Supplementary Material

Refer to Web version on PubMed Central for supplementary material.

Acknowledgments

SupportbyGrantsHL081273,EB007279, and NS031465 from the NIH is gratefully acknowledged. We thank Dr. Patrick Carroll (Department of Chemistry, University of Pennsylvania) for X-ray structure determination and Drs. Kristina Danielian and Vladimir Muzykantov (Department of Pharmacology, University of Pennsylvania) for the help with oxygen measurements in the mouse brain.

REFERENCES AND NOTES

1. Borisov SM, Klimant I. Analyst 2008;133:1302–1307. [PubMed: 18810278]
2. Fréchet, JMJ.; Tomalia, DA., editors. Dendrimers and Other Dendritic Polymers. Wiley; New York: 2001.
3. (a) Gorman CB, Smith JC. Acc Chem Res 2001;34:60. [PubMed: 11170357] (b) Hecht S, Fréchet JMJ. Angew Chem, Int Ed 2001;40:74.
4. (a) Balzani V, Ceroni P, Maestri M, Saudan C, Vicinelli V. Top Curr Chem 2003;228:159–191. (b) Ceroni P, Bergamini G, Marchioni F, Balzani V. Prog Polym Sci 2005;30:453–473.
5. (a) Vanderkooi JM, Maniara G, Green TJ, Wilson DF. J Biol Chem 1987;262:5476–5482. [PubMed: 3571219] (b) Wilson DF, Rumsey WL, Green TJ, Vanderkooi JM. J Biol Chem 1988;263:2712–2718. [PubMed: 2830260]

6. Oximetry using solid-state luminescent probes or probes in which phosphorescent chromophores are embedded in polymeric carrier nanoparticles is a large area of research (for selected examples, see refs 7 and 20). In this paper, we focus on “molecular” oxygen probes, where each sensing motif is an individual well-characterized molecule.
7. (a) Demas JN, DeGraff BA, Coleman PB. Anal Chem 1999;71:793A–800A. (b) Amao Y. Microchim Acta 2003;143:1–12. (c) Papkovsky DB, O’Riordan TC. J Fluores 2005;15:569–584.For recent examples, see: (d) Huynh L, Wang ZU, Yang J, Stoeva V, Lough A, Manners I, Winnik MA. Chem Mater 2005;17:4765–4773. (e) Fernandez-Sanchez JF, Roth T, Cannas R, Nazeeruddin MK, Spichiger S, Graetzel M, Spichiger-Keller UE. Talanta 2007;71:242–250. [PubMed: 19071295] (f) Borisov SM, Klimant I. Anal Chem 2007;79:7501–7509. [PubMed: 17718539] (g) Borisov SM, Nuss G, Klimant I. Anal Chem 2008;80:9435–9442. [PubMed: 19006407]
8. (a) Pawlowski M, Wilson DF. Adv Exp Med Biol 1992;316:179–182. [PubMed: 1288078] (b) Rumsey WL, Vanderkooi JM, Wilson DF. Science 1988;241:1649–1651. [PubMed: 3420417] (c) Shonat RD, Wilson DF, Riva CE, Pawlowski M. Appl Opt 1992;33:3711–3718. (d) Wilson DF, Cerniglia G. Cancer Res 1992;52:3988–3993. [PubMed: 1617675] For more recent examples, see: (e) Kindig CA, Kelley KM, Howlett RA, Stary CM, Hogan MC. J Appl Physiol 2003;94:353–357. [PubMed: 12391049] (f) Ferreira LF, McDonough P, Behnke BJ, Musch TI, Poole DC. Respir Physiol Neurobiol 2006;153:237–249. [PubMed: 16376620] (g) Johannes T, Mik EG, Nohe B, Unertl KE, Ince C. Am J Physiol Ren Physiol 2007;292:F796–F803. (h) Golub AS, Pittman RN. Am J Physiol Heart Circ Physiol 2008;294:H2905–H2916. [PubMed: 18375716]
9. Finikova OS, Lebedev AY, Aprelev A, Troxler T, Gao F, Garnacho C, Muro S, Hochstrasser RM, Vinogradov SA. ChemPhysChem 2008;9:1673–1679. [PubMed: 18663708]
10. Apreleva SV, Wilson DF, Vinogradov SA. Appl Opt 2006;45:8547–8559. [PubMed: 17086268]
11. Koch, CJ. Redox Cell Biology and Genetics. Vol. 352. Elsevier; New York: 2002. p. 3-31.
12. Swartz HM, Clarkson RB. Phys Med Biol 1998;43:1957–1975. [PubMed: 9703059]
13. Krishna MC, English S, Yamada K, Yoo J, Murugesan R, Devasahayam N, Cook JA, Golman K, Ardenkjaer-Larsen JH, Subramanian S, Mitchell JB. Proc Natl Acad Sci USA 2002;99:2216–2221. [PubMed: 11854518]
14. Jobsis FF. Science 1977;198:1264–1267. [PubMed: 929199]
15. (a) Ziemer LS, Evans SM, Kachur A, Shuman AL, Cardi CA, Jenkins WT, Karp JS, Alavi A, Dolbier WR, Koch CJ. Eur J Nucl Med Mol Imaging 2003;30:259–266. [PubMed: 12552344] (b) Tatum JL, Kelloff GJ, Gillies RJ. Int J Radiat Biol 2006;82:699–757. [PubMed: 17118889]
16. Sibrian-Vazquez M, Jensen TJ, Vicente MGH. J Photochem Photobiol, B 2007;86:9–21. [PubMed: 16987669]
17. (a) Vinogradov SA, Wilson DF. Adv Exp Med Biol 1997;428:657–662. [PubMed: 9500112] (b) Vinogradov SA, Lo LW, Wilson DF. Chem—Eur J 1999;5:1338–1347. (c) Rietveld IB, Kim E, Vinogradov SA. Tetrahedron 2003;59:3821–3831.
18. (a) Dunphy I, Vinogradov SA, Wilson DF. Anal Biochem 2002;310:191–198. [PubMed: 12423638] (b) Thompson JK, Peterson MR, Freeman RD. Science 2003;299:1070–1072. [PubMed: 12586942] (c) Poole DC, Behnke BJ, McDonough P, McAllister RM, Wilson DF. Microcirculation 2004;11:317–326. [PubMed: 15280071] (d) Pirow R, Baumer C, Paul RJ. J Exp Biol 2004;207:4393–4405. [PubMed: 15557025] (e) Wilson DF, Lee WMF, Makonnen S, Finikova O, Apreleva S, Vinogradov SA. J Appl Physiol 2006;101:1648–1656. [PubMed: 16888050] (f) Johannes T, Mik EG, Ince C. J Appl Physiol 2006;100:1301–1310. [PubMed: 16357065]
19. Estrada AD, Ponticorvo A, Ford TN. Opt Lett 2008;33:1038–1040. [PubMed: 18483504]
20. (a) Xu H, Aylott JW, Kopelman R, Miller TJ, Philbert MA. Anal Chem 2001;73:4124–4133. [PubMed: 11569801] (b) Ji J, Rosenzweig N, Jones I, Rosenzweig Z. Anal Chem 2001;73:3521–3527. [PubMed: 11510813] (c) Koo YEL, Cao YF, Kopelman R, Koo SM, Brasuel M, Philbert MA. Anal Chem 2004;76:2498–2505. [PubMed: 15117189] (d) Han BH, Winnik MA, Bourlinos AB, Giannelis EP. Chem Mater 2005;17:4001–4009. (e) Zhang HD, Sun YH, Ye KQ, Zhang P, Wang Y. J Mater Chem 2005;15:3181–3186. (f) Guice KB, Caldorera ME, McShane MJ. J Biomed Opt 2005;10:064031. [PubMed: 16409096] (g) Schmalzlin E, van Dongen JT, Klimant I, Marmodee B, Steup M, Fisahn J, Geigenberger P, Lohmannsroben HG. Biophys J 2005;89:1339–1345. [PubMed: 16049223]
21. Turro, NJ. Modern Molecular Photochemistry. University Science Books; Sausalito, CA: 1991.

22. At 298 K and an air pressure of 760 mmHg (oxygen fraction in the air is 21% or 159.6 mmHg), air-equilibrated aqueous solutions are 252 μM in O_2 (Fogg, PGT.; Gerrard, W. Solubility of gases in liquids. Wiley; New York: 2001.).
23. Eastwood D, Gouterman M. J Mol Spectrosc 1970;35:359–375.
24. Kim DH, Holten D, Gouterman M, Buchler JW. J Am Chem Soc 1984;106:4015–4017.
25. Morris KJ, Roach MS, Xu WY, Demas JN, DeGraff BA. Anal Chem 2007;79:9310–9314. [PubMed: 17985845]
26. The "brightness" of the chromophore is defined as the product of the molar extinction coefficient and the emission quantum yield.
27. DeRosa MC, Mosher PJ, Yap GPA, Focsaneanu KS, Crutchley RJ, Evans CEB. Inorg Chem 2003;42:4864–4872. [PubMed: 12895108]
28. (a) Vinogradov SA, Wilson DF. J Chem Soc, Perkin Trans 2;1995:103–111. (b) Vinogradov SA, Lo LW, Jenkins WT, Evans SM, Koch C, Wilson DF. Biophys J 1996;70:1609–1617. [PubMed: 8785320]
29. Papkovsky DB, Ponomarev GV, Wolfbeis OS. Spectrochim Acta, Part A 1996;52:1629–1638.
30. Zhang G, Chen J, Payne SJ, Kooi SE, Demas JN, Fraser CL. J Am Chem Soc 2007;129:8942. [PubMed: 17608480]
31. (a) Finikova O, Cheprakov A, Beletskaya I, Vinogradov S. Chem Commun 2001:261–262. (b) Finikova OS, Cheprakov AV, Carroll PJ, Vinogradov SA. J Org Chem 2003;68:7517–7520. [PubMed: 12968910] (c) Finikova OS, Cheprakov AV, Beletskaya IP, Carroll PJ, Vinogradov SA. J Org Chem 2004;69:522–535. [PubMed: 14725469] (d) Finikova OS, Aleshchenkov SE, Briñas RP, Cheprakov AV, Carroll PJ, Vinogradov SA. J Org Chem 2005;70:4617–4628. [PubMed: 15932297] (e) Finikova OS, Cheprakov AV, Vinogradov SA. J Org Chem 2005;70:9562–9572. [PubMed: 16268634] (f) Filatov MA, Lebedev AY, Vinogradov SA, Cheprakov AV. J Org Chem 2008;73:4175–4185. [PubMed: 18452337]
32. (a) Tsvirko MP, Sapunov VV, Soloviyev KN. Opt Spektrosk 1973;34:1094–1100. (b) Rozhkov VV, Khajehpour M, Vinogradov SA. Inorg Chem 2003;42:4253–4255. [PubMed: 12844293]
33. (a) Borek C, Hanson K, Djurovich PI, Thompson ME, Aznavour K, Bau R, Sun YR, Forrest SR, Brooks J, Michalski L, Brown J. Angew Chem, Int Ed 2007;46:1109–1112. (b) Sommer JR, Farley RT, Graham KR, Yang Y, Reynolds JR, Xue J, Schanze KS. ACS Appl Mater Interfaces 2009;1:274–278.
34. *meso*-Tetraarylated porphyrins, tetrabenzoporphyrins, and tetranaphthoporphyrins are usually abbreviated as Ar_4P, Ar_4TBP, and Ar_4TNP, respectively, in order to distinguish them from *meso*-unsubstituted analogues. In the present paper, we used only *meso*-tetrarylated macrocycles, and therefore we omit the prefix "Ar_4".
35. (a) Knyukshto VN, Sagun EI, Shul'ga AM, Bachilo SM, Starukhin DA, Zen'kevich EI. Opt Spectrosk 2001;90:67. (b) Knyukshto VN, Shul'ga AM, Sagun EI, Zen'kevich EI. Opt Spectrosk 2002;92:53. (c) Knyukshto VN, Shul'ga AM, Sagun EI, Zen'kevich EI. Opt Spectrosk 2006;100:590–601.
36. Lebedev AY, Filatov MA, Cheprakov AV, Vinogradov SA. J Phys Chem A 2008;112:7723–7733. [PubMed: 18665576]
37. Seybold PG, Gouterman M. J Mol Spectrosc 1969;31:1.
38. Taroni P, Pifferi A, Torricelli A, Comelli D, Cubeddu R. Photochem Photobiol Sci 2003;2:124–129. [PubMed: 12664972]
39. Tripathy U, Kowalska D, Liu X, Velate S, Steer RP. J Phys Chem A 2008;112:5824–5833. [PubMed: 18537232]
40. Lindsey JS, Schreiman IC, Hsu HC, Kearney PC, Marguerettaz AM. J Org Chem 1987;52:827–836.
41. (a) Arnold DP, Burgess-Dean L, Hubbard J, Abdur Rahman M. Aust J Chem 1994;47:969–974. (b) Abel Y, Haake E, Haake G, Schmidt W, Struve D, Walter A, Montforts FP. Helv Chim Acta 1998;81:1978–1996.
42. For examples, see: (a) Jin RH, Aida T, Inoue S. J Chem Soc, Chem Commun 1993:1260–1262. (b) Sadamoto R, Tomioka N, Aida T. J Am Chem Soc 1996;118:3978–3979. (c) Kimura M, Nakada K, Yamaguchi Y, Hanabusa K, Shirai H, Kobayashi N. Chem Commun 1997:1215–1216. (d) Issberner J, Vögtle F, DeCola L, Balzani V. Chem—Eur J 1997;3:706–712. (e) Vögtle F, Plevoets M, Nieger M, Azzellini GC, Credi A, De Cola L, De Marchis V, Venturi M, Balzani V. J Am Chem Soc

1999;121:6290–6298. (f) Riley JM, Alkan S, Chen AD, Shapiro M, Khan WA, Murphy WR, Hanson JE. Macromolecules 2001;34:1797–1809.

43. Rozhkov V, Wilson D, Vinogradov S. Macromolecules 2002;35:1991–1993.
44. Khajehpour M, Rietveld I, Vinogradov S, Prabhu NV, Sharp KA, Vanderkooi JM. Proteins: Struct, Funct, Genet 2003;53:656–666. [PubMed: 14579357]
45. Vinogradov SA. Org Lett 2005;7:1761–1764. [PubMed: 15844900]
46. Caliceti P, Veronese FM. Adv Drug Delivery Rev 2003;55:1261–1277.
47. Gajbhiye V, Kumar PV, Tekade RK, Jain NK. Curr Pharm Des 2007;13:415–429.
48. Guillaudeu SJ, Fox ME, Haidar YM, Dy EE, Szoka FC, Fréchet JMJ. Bioconjugate Chem 2008;19:461–469.
49. Dichtel WR, Baek KY, Fréchet JMJ, Rietveld IB, Vinogradov SA. J Polym Sci, Part A: Polym Chem 2006;44:49394951.
50. Kaminski ZJ. Biopolymers 2000;55:140–164. [PubMed: 11074411]
51. Han SY, Kim YA. Tetrahedron 2004;60:2447–2467.
52. Biechler SS, Taft RW. J Am Chem Soc 1957;79:4927–4935.
53. Dandliker, PJ.; Diederich, F.; Gross, M.; Knobler, CB.; Louati, A.; Sanford, EM. Angew Chem, Int Ed. Vol. 33. 1994. p. 1739-1742. (b) Dandliker PJ, Diederich F, Gisselbrecht JP, Louati A, Gross M. Angew Chem, Int Ed 1996;34:2725–2728.
54. While this paper was in preparation, an article appeared in press (ref 33b) reporting independently on the photophysical properties of platinum tetraphenyltetranaphthoporphyrin.
55. The plots of Pt-1-OPEG and 8 display lower k_q values than they would be expected to display in the absence of aggregation.
56. In separate experiments, we have established that dendritic probes do not permeate cellular membranes and that the presence of erythrocytes has no effect on the calibration constants.
57. Vinogradov SA, Fernandez-Seara MA, Dugan BW, Wilson DF. Rev Sci Instrum 2001;72:3396–3406.
58. (a) Marshall WH. Physiol Rev 1959;39:239–279. [PubMed: 13645235] (b) Ayata C, Shin HK, Salomone S, Ozdemir-Gursoy Y, Boas DA, Dunn AK, Moskowitz MA. J Cereb Blood Flow Metab 2004;24:1172–1182. [PubMed: 15529018] (c) Sakadžić S, Yuan S, Dilekoz E, Ruvinskaya S, Vinogradov SA, Ayata C, Boas DA. Appl Opt. 2009 in press.
59. Hadjikhani N, Sanchez Del Rio M, Wu O, Schwartz D, Bakker D, Fischl B, Kwong KK, Cutrer FM, Rosen BR, Tootell RB, Sorensen AG, Moskowitz MA. Proc Natl Acad Sci USA 2001;98:4687–4692. [PubMed: 11287655]
60. Nedergaard M. Acta Neurol Scand 1988;77:81–101. [PubMed: 3284272]
61. Khajehpour M, Rietveld I, Vinogradov S, Prabhu NV, Sharp KA, Vanderkooi JM. Proteins: Struct, Funct, Genet 2003;53:656–666. [PubMed: 14579357]

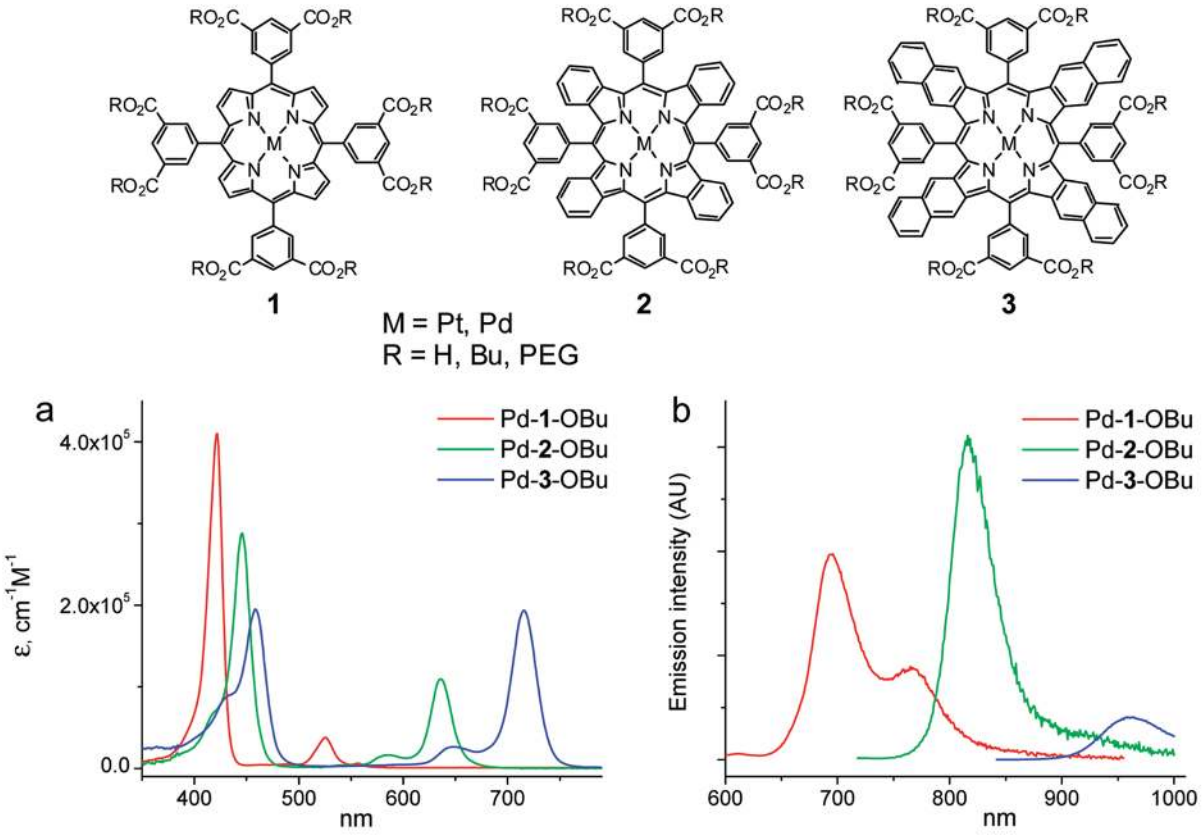

FIGURE 1.

Three basic structural types of porphyrins that are used as sensing elements of phosphorescent probes. [PEG refers to monomethoxy-oligo(ethylene glycol); av MW 350.] Absorption and emission spectra of complexes Pd-1-OBu, Pd-2-OBu, and Pd-3-OBu in benzonitrile (PhCN) are shown.

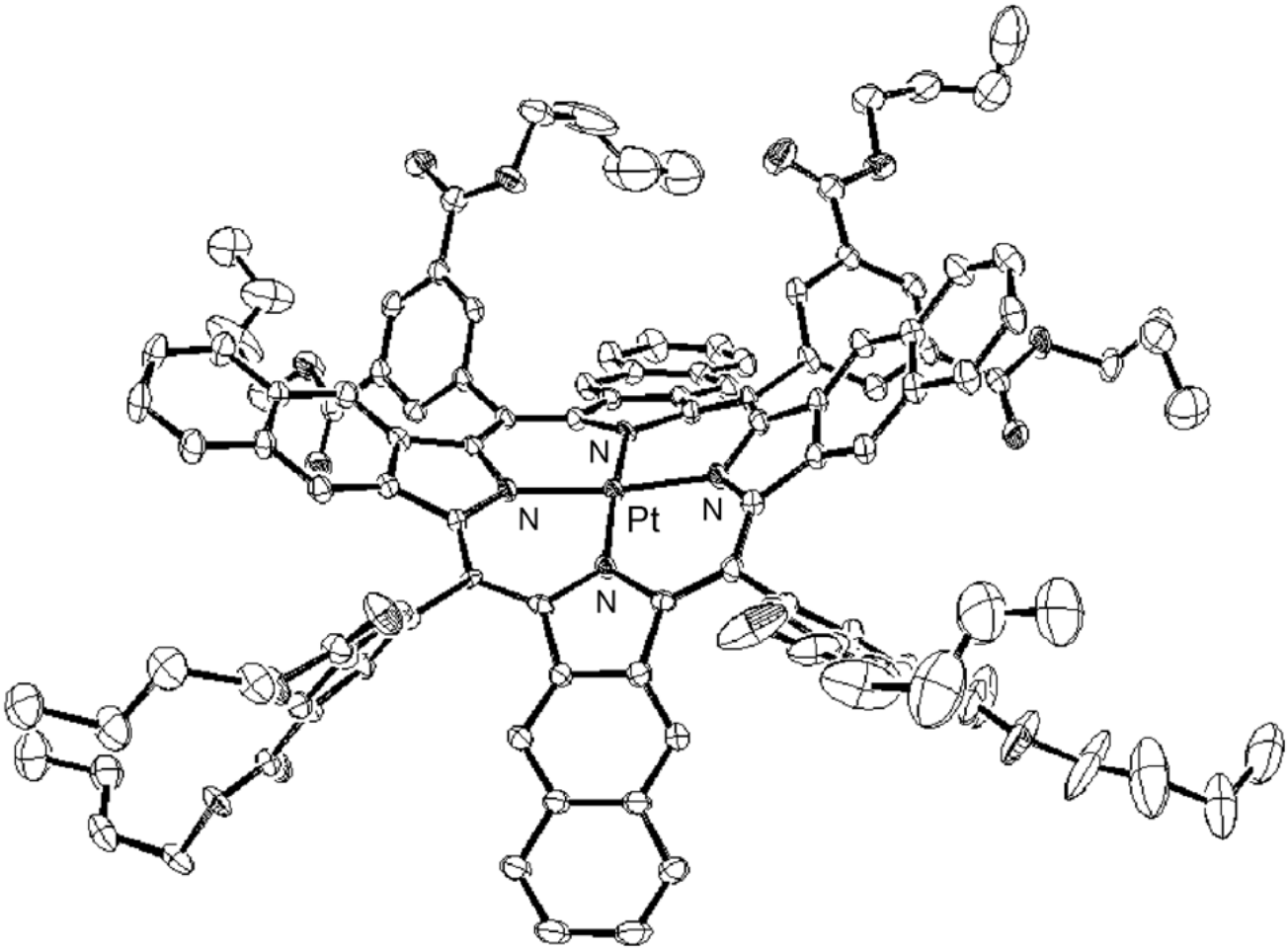

FIGURE 2.
X-ray crystal structure of Pt-3-Bu.

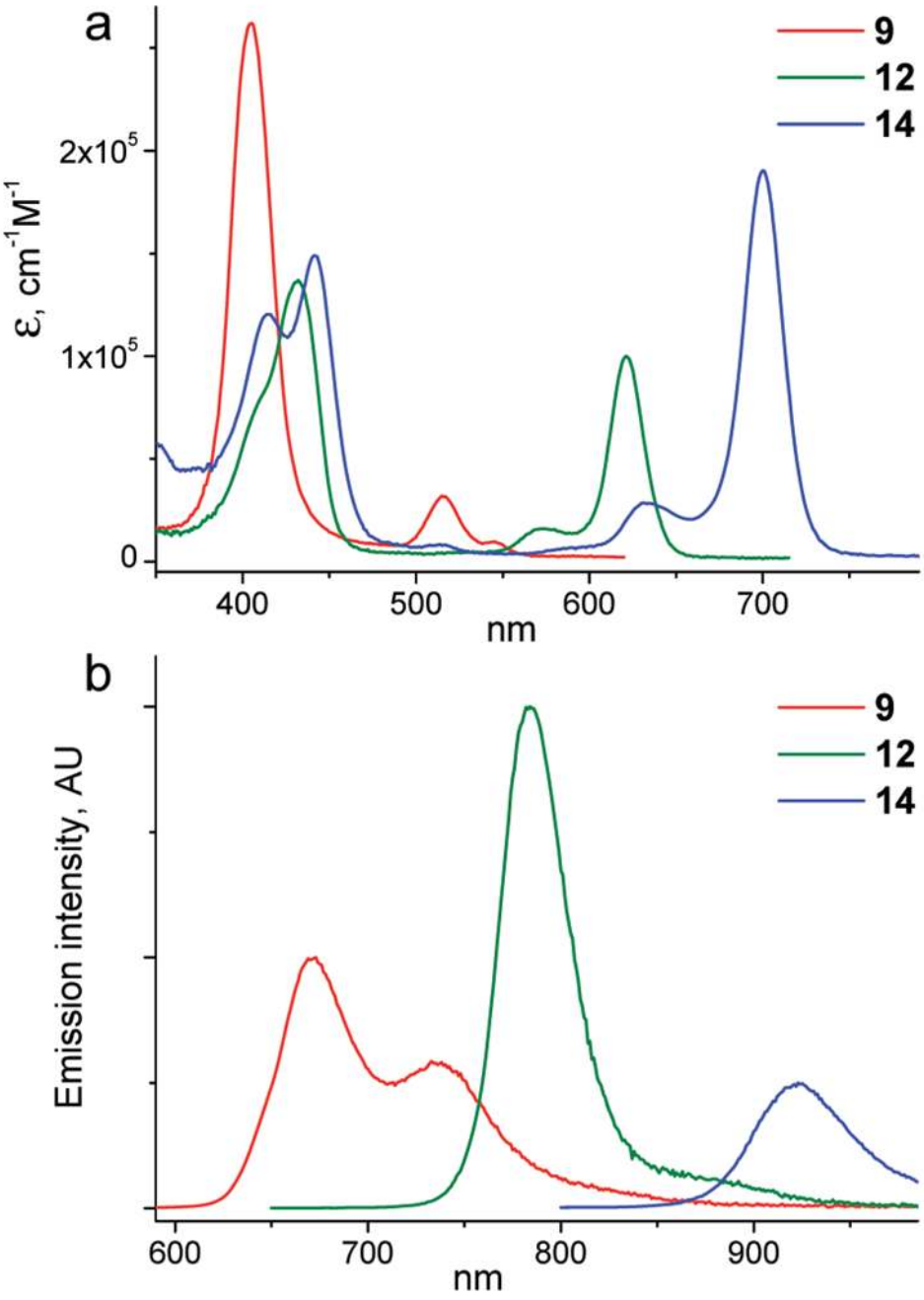

FIGURE 3.

Absorption (a) and emission (b) spectra in water of the G2 dendrimers based on platinum porphyrins with increasing degrees of π-conjugation. The emission spectra are scaled to reflect the relative phosphorescence quantum yields in the absence of quenching.

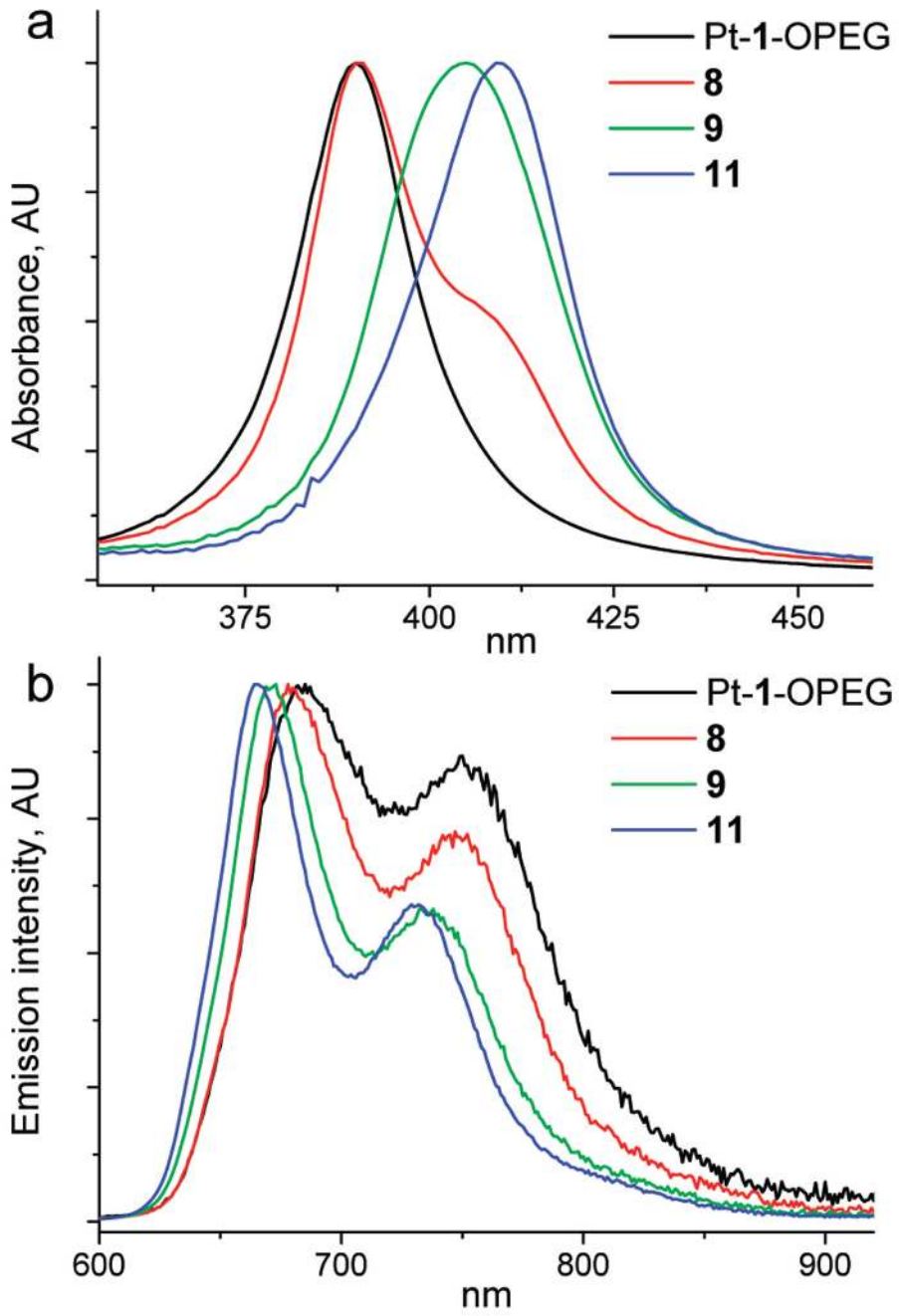

FIGURE 4.
Changes in the absorption (a) and phosphorescence (b) spectra (in water) of platinum porphyrin-based dendrimers with the generation number.

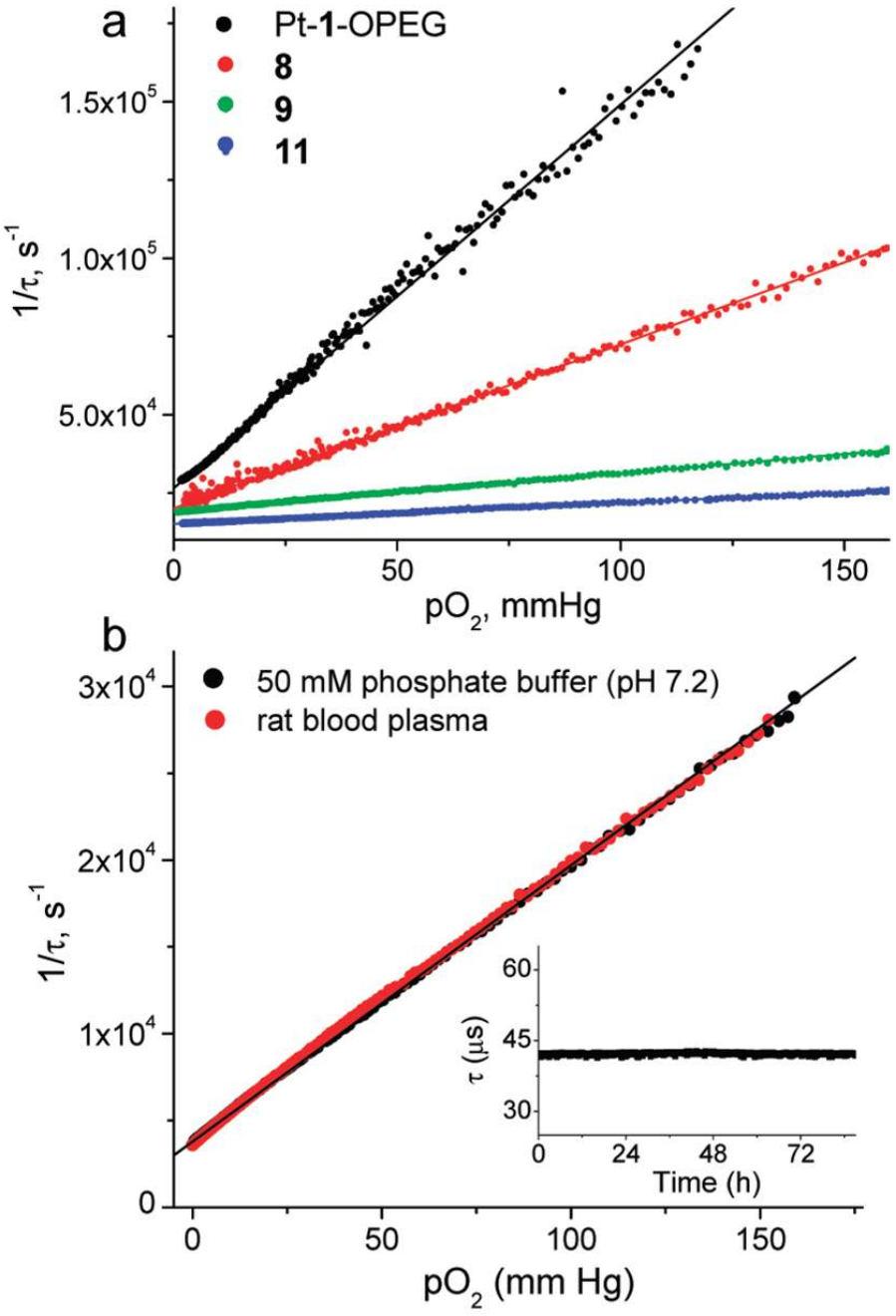

FIGURE 5.

(a) Stern–Volmer oxygen quenching plots of platinum porphyrin dendrimers in a 50 mM phosphate buffer, pH 7.4, 23 °C. The solid lines show the fits of the data to the Stern–Volmer equation (2). (b) Stern–Volmer plots of probe 13 in a 50 mM phosphate buffer solution and in rat blood at 36.9 °C. To prevent coagulation, the blood was treated with heparin. Inset: Measurements at air saturation at 22 °C were taken at 10 min intervals over 80 h.

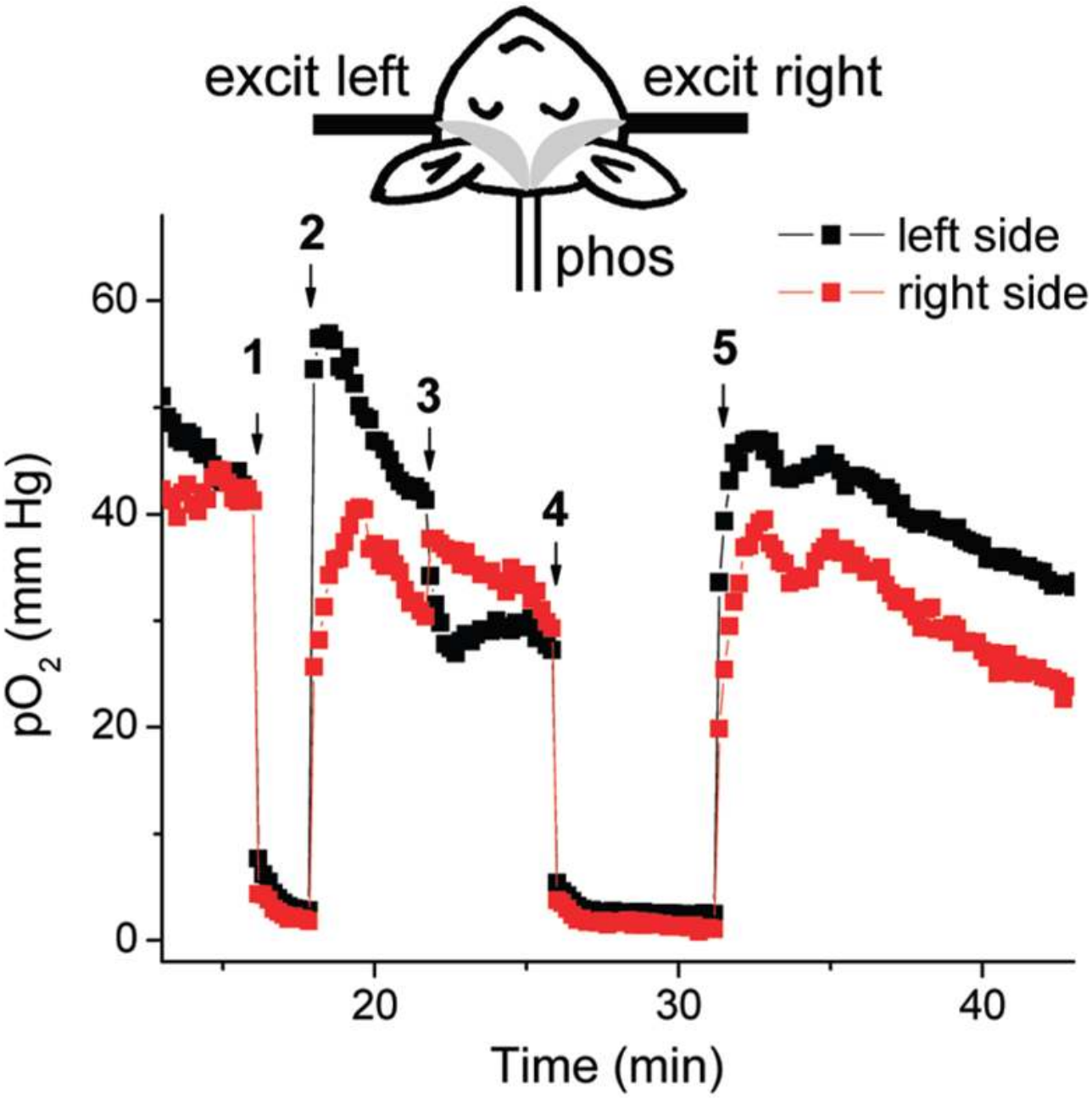

FIGURE 6.

Time traces of pO_2 values in two hemispheres of the mouse brain measured using probe 13. Excitation was delivered by the fibers positioned on the right and left sides of the scull. Phosphorescence was collected by the bottom fiber. Gray shapes in the schematics show the sampled optical paths: 1 and 4, occlusion of both carotid arteries; 3, occlusion of the left carotid artery only; 2 and 5, reperfusion.

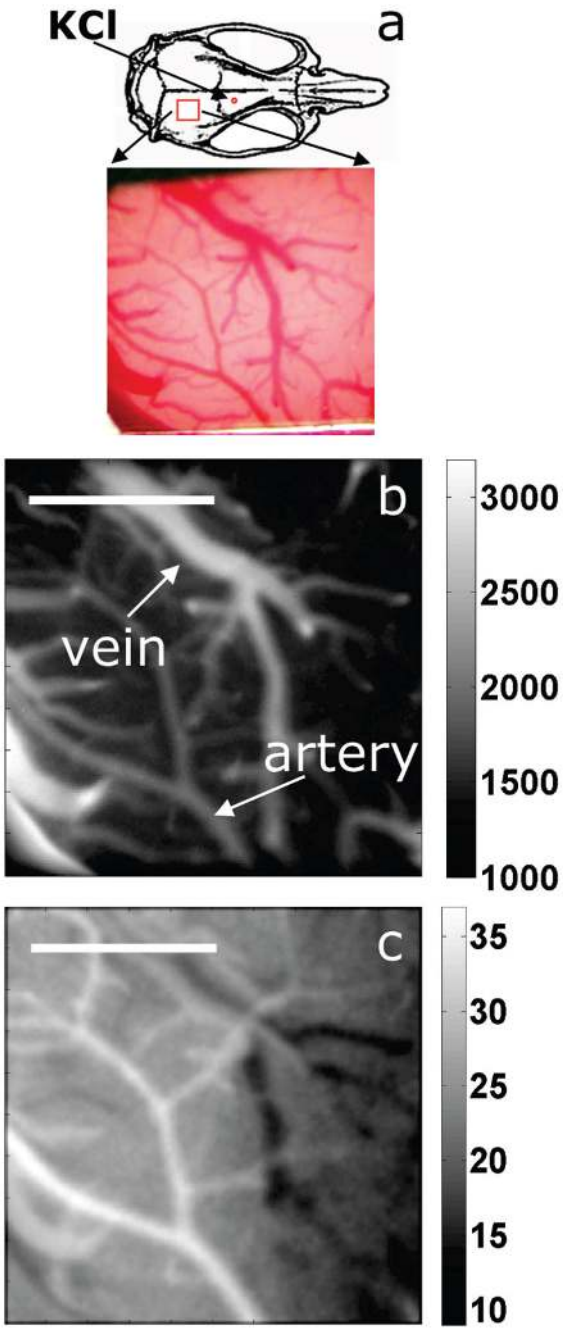

FIGURE 7.

Imaging of pO_2 in cortical vasculature. (a) The position of the cranial window and the location of KCl injection are marked on the schematic of the rat skull. The photograph of the cortical vasculature was taken through the microscope eyepiece. (b) Phosphorescence intensity (AU) image. Arteries and veins were recognized based on their morphological details. (c) pO_2 (mmHg) image before arrival of the CSD. Scale bar: 1 mm.

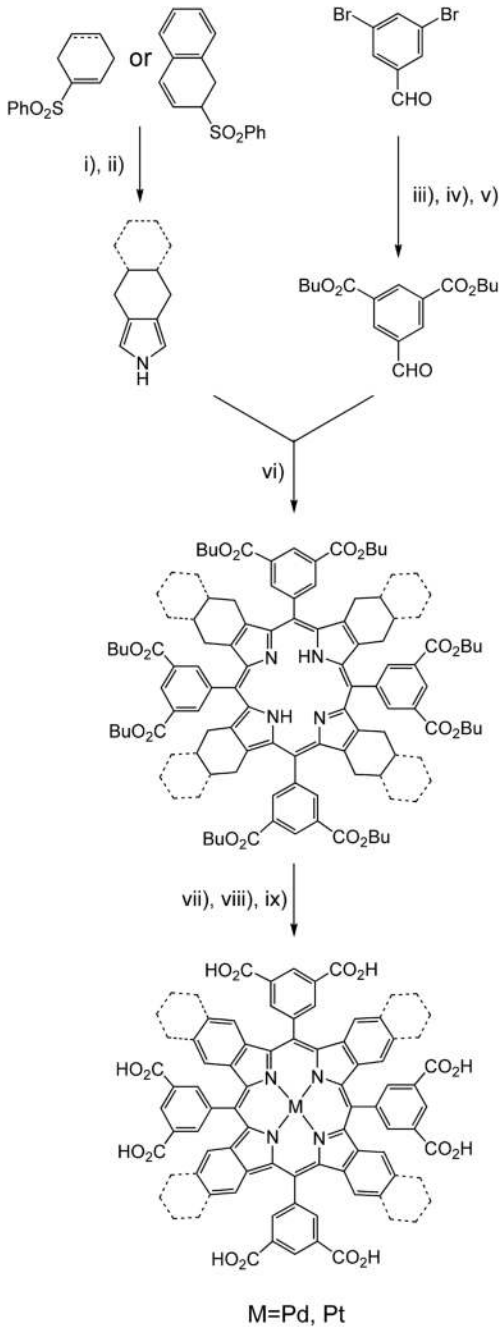

Scheme 1. Synthesis of Pd and Pt Complexes of TBPs and TNPs[a]

[a] TNPs and the corresponding precursors are shown with dashed lines: (i) modified Barton–Zard reaction with ethyl isocyanoacetate (41); (ii) hydrolysis/decarboxylation (31b); (iii) protection of the aldehyde with 1,3-propanediol (31d); (iv) Pd^0-catalyzed butoxycarbonylation (31d); (v) deprotection by THF/HCl (31d); (vi) Lindsey condensation (40); (vii) metal insertion (31b, 31d); (viii) oxidative aromatization with DDQ (31b, 31d); (xi) base-mediated hydrolysis.

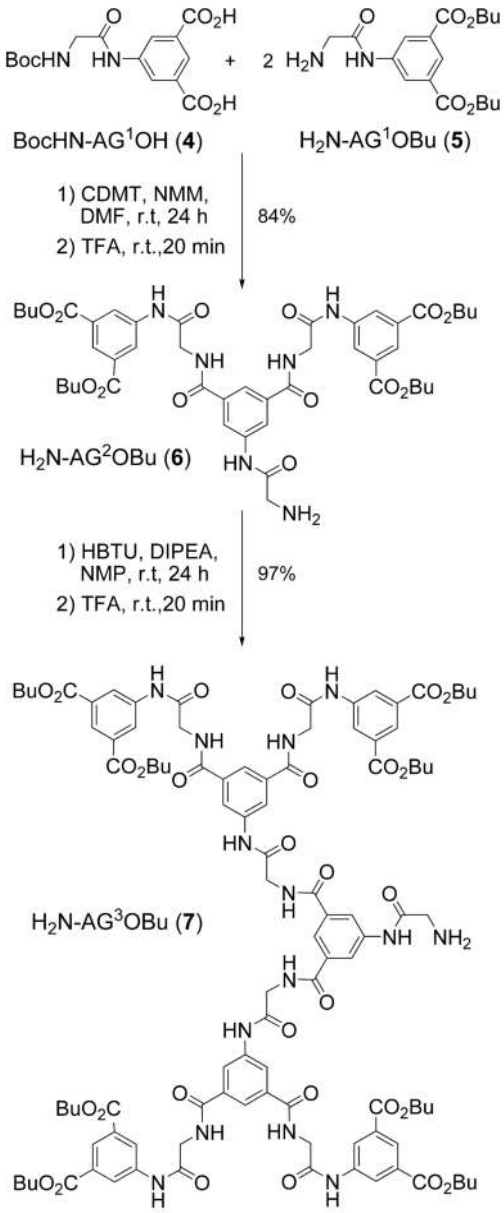

Scheme 2. Synthesis of AG Dendrons[a]

[a] CDMT = 2-chloro-4,6-dimethoxy-1,3,5-triazine; NMM = *N*-methylmorpholine; HBTU = *o*-benzotriazole-*N*,*N*,*N*′,*N*′-tetramethyluronium hexafluorophosphate; DIPEA = *N*,*N*-diisopropylethylamine.

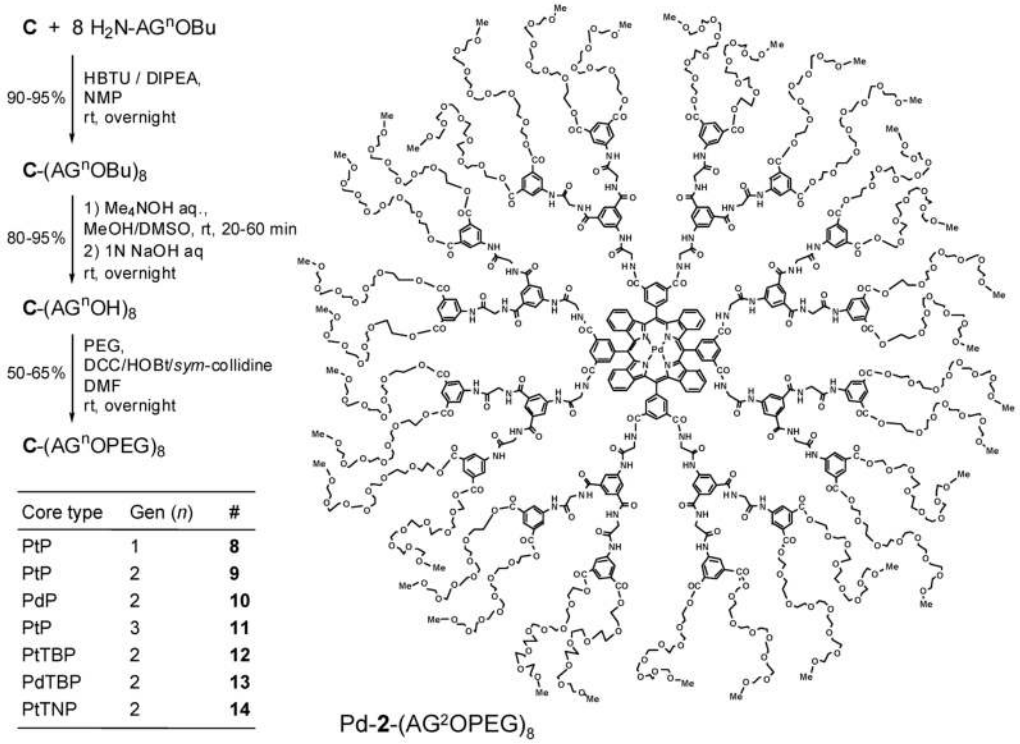

Core type	Gen (*n*)	#
PtP	1	**8**
PtP	2	**9**
PdP	2	**10**
PtP	3	**11**
PtTBP	2	**12**
PdTBP	2	**13**
PtTNP	2	**14**

Scheme 3. Dendrimer Synthesis and Modification[a]

[a] In the first line, **C** (core) designates porphyrin octacarboxylic acids: Pt-**1**-OH, Pd-**1**-OH, Pt-**2**-OH, Pd-**2**-OH, Pd-**3**-OH. The table shows the numbering scheme for probes of the general formula **C**-(AG^{2}OPEG)$_8$. HOBt = *N*-hydroxybenzotriazole; PEG = oligo(ethylene glycol) monomethyl ether; av MW 350.

Table 1

Photophysical Properties of Pt and Pd Complexes of P, TBP, and TNP

	absorption		phosphorescence[a]	
metalloporphyrin	Soret band, nm (log ε, M^{-1} cm^{-1})	*Q* band, nm (log ε, M^{-1} cm^{-1})	λ_{max}, nm	φ/τ_0,[b] μs
Pd-**1**-OBu	422 (5.61)	526 (4.57)	696	0.08/504
Pd-**2**-OBu	446 (5.46)	635 (5.00)	816	0.09/210
Pd-**3**-OBu	458 (5.29)	716 (5.29)	961[c]	0.02[c]/52

[a] Measured using a solution in PhCN at 22 °C, deoxygenated by argon bubbling.

[b] Emission quantum yields were determined relative to the fluorescence of H_2TPP (φ_{fl} = 0.11) (37) in deoxygenated benzene.

[c] Measurements above 900 nm are subject to large experimental errors because of the very low quantum efficiency of the detection systems in the red part of the spectrum.

Table 2

Photophysical Properties of the Phosphorescent Probes

		absorption		phosphorescence[c]				
generation	**compound**	**λ, nm**		**λ_{max}, nm**	**φ**	**τ_0, μs**	**k_q,[b] mmHg^{-1} s^{-1}**	**R[e]**
0	Pt-**1**-OBu[a]	405	511	664	0.23	53		
0	Pt-**1**-OPEG[b]	389	520	682	0.05	37	1208 ± 15	0.88
1	**8**[b]	390	520	681	0.09	48	521 ± 3; 521 ± 3[d]	0.80
2	**9**[b]	398	516	671	0.14	53	120 ± 3; 120 ± 3[d]	0.50
2	**10**[b]	403	532	708	0.07	720	97 ± 4	0.92
3	**11**[b]	409	515	664	0.18	66	66.6 ± 0.2	0.41
0	Pt-**2**-OBu[a]	432	621	791	0.30	41		
2	**12**[b]	432	621	791	0.24	54	171 ± 5	0.59
2	**13**[b]	446	635	816	0.03	270	122 ± 5	0.84
0	Pt-**3**-OBu[a]	442	699	922	0.07	12		
2	**14**[b]	442	699	923	0.06	11	163 ± 10	0.22

[a] Measured using a ~2 μM solution of the probe in PhCN.

[b] Measured using a ~2 μM solution of the probe in a 50 mM phosphate buffer, pH = 7.4, 23 °C.

[c] Deoxygenated by argon bubbling (PhCN solutions) or using the glucose/glucose oxidase/catalase system (aqueous solutions) (5).

[d] Measured in the presence bovine serum albumin (1%).

[e] Dynamic range parameter: $R = (\tau_0 - \tau_{air})/\tau_0$, where τ_0 (pO_2 = 0 mmHg) and τ_{air} (pO_2 = 159.6 mmHg).